Probabilistic Risk Assessment of Electric Power Infrastructure Subjected to Earthquake-Induced Landslides

Ezra Jampole, Ph.D., P.E.
Senior Managing Engineer, Buildings and Structures, Exponent, New York, New York, USA

Maha Kenawy, Ph.D.
Associate, Buildings and Structures, Exponent, Menlo Park, California, USA

ABSTRACT: We develop a probabilistic framework to assess the vulnerability of electric power transmission structures to shallow landslides induced by earthquake ground shaking. We probabilistically describe possible damage states of transmission pole structures that may be induced by differential ground movement during landslide events, as a function of their configuration, material properties, and connectivity to electrical overhead conductors. We integrate the fragilities of the structures with the earthquake-induced landslide displacement hazard, which is predicted based on the geotechnical site properties using a Newmark sliding block model, and the seismic hazard at the site obtained via probabilistic seismic hazard analysis. Accordingly, we predict annual rates of failure based on the deformation of the structures due to ground movement. The framework is implemented at a regional scale utilizing the U.S. Geological Survey's seismic hazard disaggregation tool and the underlying U.S. National Seismic Hazard Map to quantify the risks to electric power infrastructure due to earthquake-induced landslide hazards.

1. INTRODUCTION

Earthquake ground shaking can cause slope instability and lead to the occurrence of landslides, which are typically associated with substantial economic losses. For example, the 1994 Northridge earthquake in California triggered more than 11,000 landslides which damaged or destroyed dozens of structures (Jibson and Harp 1995), and the 1999 Chi-Chi earthquake in Taiwan is estimated to have triggered over 20,000 landslides (Lin et al. 2004). Lifeline infrastructure may be vulnerable to a disruption of function, damage, or failure under the impacts of earthquake events in regions of high seismic hazard levels, due to ground shaking or geohazards induced by the earthquake shaking such as landslides. Figure 1 shows an example of movement due to a landslide during the 2023 Kahramanmaraş earthquake in Turkey, which caused differential movement of the legs of a transmission tower, and resulted in collapse. Understanding the consequences of earthquake-induced landslides on lifeline infrastructure is critical for hazard preparedness, disaster emergency response, and increasing overall community resilience to earthquakes.

Figure 1. Earthquake-induced landslide causing differential displacement of the legs of an electric transmission tower and collapse, from the 2023 M7.8 Kahramanmaraş Earthquake.

In this study, we develop a probabilistic risk model to assess the vulnerability of electric power structures to earthquake-induced landslides based on the framework of probabilistic seismic hazard analysis. We focus the discussion on wood poles

as the specific type of electric utility structure. We calculate the deformation of the wood poles caused by a change in the tension of the electric overhead conductors, induced by a landslide moving the base of the pole relative to adjacent poles. Annual rates of exceeding a leaning limit state for the pole are calculated by integrating the pole fragility with site-specific landslide displacement hazard curves.

2. SYSTEM DEFINITION

Landslides may move wood poles relative to the location of adjacent wood poles in a power line. This movement will cause the spans between the wood poles to change in direction and/or length, thus the tension in the conductors between the poles will change, potentially increasing the bending stresses at the pole base. It is conservatively assumed that all landslides differentially move a wood pole directly parallel to a tangent line, as this has the largest effect on groundline stresses. The deformation of the top of the wood pole is used as a proxy for pole lean. We also assume that there is no slippage at the conductor clamps or failure of conductor splices.

Figure 2 shows a typical system prior to a landslide: L_1 and L_2 are the spans between each set of poles; T_1 and T_2 are the conductor tension forces at the external supports; H_1 and H_2 are the horizontal components of tension; and V_1 and V_2 are the vertical components of tension at the external supports in each conductor. The variables ℓ_1 and ℓ_2 are the arc lengths of the conductors in the left and right spans, respectively.

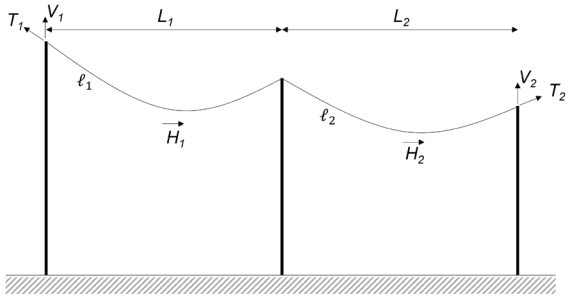

Figure 2. System prior to landslide

Figure 3 shows the system after a landslide, accounting for both the movement of the base of the pole caused by the landslide and the bending of the central pole. It is assumed that poles on either side of the pole subjected to the landslide do not move as a result of either the landslide directly or from changes in the tension in the conductors. The new spans between the poles are therefore $L_1 + \Delta_{LS} - \Delta_{pole}$ and $L_1 - \Delta_{LS} + \Delta_{pole}$ where Δ_{LS} is the landslide ground displacement and Δ_{pole} is the deformation at the top of the central pole that is induced by the landslide. The updated conductor tension forces are indicted by primes ($'$) on variable names. It is assumed that the arc length of conductor in each span remains unchanged.

Figure 4 shows a schematic diagram of a wood pole: h_0 is the diameter of the pole top; a is the ratio of the diameter at the ground line to the diameter and the pole top; L is the height of the pole (up to the conductor attachment point); and δH_1 and δH_2 are the changes in the horizontal component of tension in the left and right spans, respectively:

$$\delta H_1 = (H_1' - H_1)n_1 \quad (1)$$

$$\delta H_2 = (H_2' - H_2)n_2 \quad (2)$$

where n_1 and n_2 are the number of conductors in each span. The diameter of the pole, $h(x)$, and the moment of inertial of the pole, $I(x)$, are defined for any point along the pole as follows:

$$h(x) = ah_0 - \frac{(a-1)h_0}{L} \cdot x \quad (3)$$

$$I(x) = \frac{\pi}{64}\left[ah_0 - \frac{(a-1)h_0}{L} \cdot x\right]^4 \quad (4)$$

The stiffness of the pole k is calculated using the Principle of Virtual Displacements as the inverse of the pole flexibility:

$$f = \int_0^L \frac{(L-x)^2}{E\frac{\pi}{64}\left[ah_0 - \frac{(a-1)h_0}{L} \cdot x\right]^4} dx \quad (5)$$

To account for the epistemic uncertainty associated with the stiffness of the pole, the stiffnesses is assumed to be lognormally distributed with a dispersion parameter, β_k and median value $k = 1/f$.

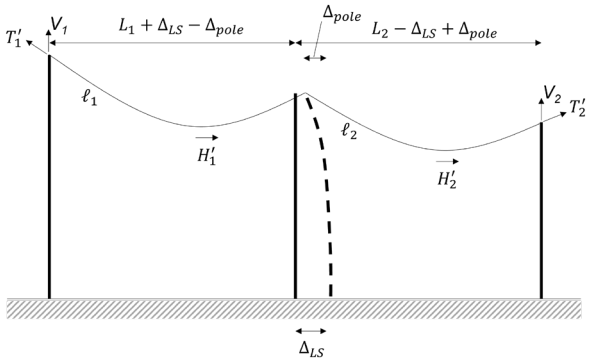

Figure 3. System after landslide.

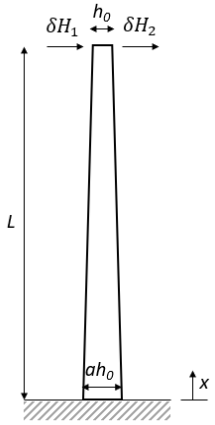

Figure 4. Diagram of wood pole.

3. POLE DEFORMATION

We estimate the deformation and stresses in a wood pole caused by the landslide movement. First, the tension in each conductor is defined based on the horizontal and vertical component of the tension. At the supports:

$$T^2 = H^2 + V^2 \tag{6}$$

Where T is the tension in the conductor, H is its horizontal component, and V is its vertical component. The vertical force in a conductor at each support assuming a level span is:

$$V = w\frac{\ell}{2} \tag{7}$$

Where ℓ is the arclength of the conductor and w is the weight per unit length of the conductor. The arc length of each conductor is calculated assuming the conductors are inextensible catenaries:

$$\ell = \frac{2H}{w}\sinh\left(\frac{wL}{2H}\right) \tag{8}$$

where H is the horizontal component of tension and L is the span between the poles. In the general case of a conductor connected to two poles at different elevations, the conductor span is inclined as shown in Figure 5, and the location of the lowest point is not in the middle of the span. The arc length of the conductor can be computed by applying the catenary equation to each part of the conductor to the left and right of the lowest point:

$$\ell_A = \frac{H}{w}\sinh\left(\frac{wx_A}{H}\right) \tag{9}$$

$$\ell_B = \frac{H}{w}\sinh\left(\frac{wx_B}{H}\right) \tag{10}$$

where both x_B and x_A have a positive sign. The total length of the conductor is the sum of the lengths of the two segments:

$$\ell = \ell_A + \ell_B \tag{11}$$

The coordinate axes are constructed such that the y-axis passes through the lowest point in the span, and x_B and x_A are the horizontal lengths from the lowest point to the two supports. The values of x_B and x_A for each conductor can be determined by enforcing the catenary equation at each support:

$$y_B = \frac{H}{w}\cosh\left(\frac{wx_B}{H}\right) \tag{12}$$

$$y_A = \frac{H}{w}\cosh\left(\frac{wx_A}{H}\right) \tag{13}$$

and utilizing the following boundary conditions that rely on the length of the span and the difference in elevation between the supports:

$$y_B - y_A = d \tag{14}$$

$$x_B + x_A = L \tag{15}$$

Solving the four equations simultaneously yields the following expressions for x_B and x_A which can be used to obtain the arc lengths:

$$x_B = \frac{H}{w}\sinh^{-1}\left(\frac{d}{\frac{2H}{w}\sinh(\frac{wL}{2H})}\right) + L/2 \quad (16)$$

$$x_A = L - x_B \quad (17)$$

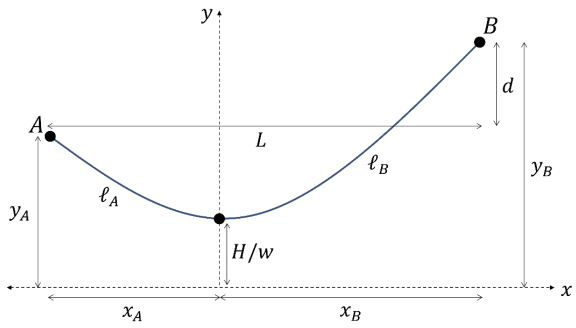

Figure 5: conductor with an inclined span.

Accordingly, the total length of each conductor is:

$$\ell = \frac{H}{w}\left(\sinh\left(\frac{wx_B}{H}\right) + \sinh\left(\frac{w(L - x_B)}{H}\right)\right) \quad (18)$$

and the vertical components of the conductor tension at each support are:

$$V_A = w\ell_A = H\sinh\left(\frac{wx_A}{H}\right) \quad (19)$$

$$V_B = w\ell_B = H\sinh\left(\frac{wx_B}{H}\right) \quad (20)$$

where ℓ_A is the arc length of the left segment of the conductor, and ℓ_B is the arc length of the right segment of the conductor. Plugging into the equation for conductor tension and utilizing the trigonometric identity $cosh^2(\theta) - sinh^2(\theta) = 1$:

$$T_A = H\cosh\left(\frac{wx_A}{H}\right) \quad (21)$$

$$T_B = H\cosh\left(\frac{wx_B}{H}\right) \quad (22)$$

where T_A and T_B are the conductor tensile forces at each support. The initial horizontal force in each conductor (H_1 and H_2) and the weight per unit length w assumed to be known, and x_A and x_B are expressed as functions of H. We assume that the arc length of each conductor does not change because of the landslide (inextensible conductors), and thus set the arc lengths before and after the landslide equal:

$$\ell_1 = \frac{H_1}{w_1}\left(\sinh\left(\frac{w_1 x_{B1}}{H_1}\right) + \sinh\left(\frac{w_1(L_1 - x_{B1})}{H_1}\right)\right) = \frac{H_1'}{w_1}\left(\sinh\left(\frac{w_1 x'_{B1}}{H_1'}\right) + \sinh\left(\frac{w_1(L_1 + \Delta_{LS} - \Delta_{pole} - x'_{B1})}{H_1'}\right)\right) \quad (23)$$

$$\ell_2 = \frac{H_2}{w_2}\left(\sinh\left(\frac{w_2 x_{B2}}{H_2}\right) + \sinh\left(\frac{w_2(L_2 - x_{B2})}{H_2}\right)\right) = \frac{H_2'}{w_2}\left(\sinh\left(\frac{w_2 x'_{B2}}{H_2'}\right) + \sinh\left(\frac{w_2(L_2 - \Delta_{LS} + \Delta_{pole} - x'_{B2})}{H_2'}\right)\right) \quad (24)$$

where the subscripts 1 and 2 refer to the conductors on either side of the pole. The spans between the poles and the horizontal forces in the conductors change because of the landslide, and x'_{B1} and x'_{B2} are computed using the new spans and horizontal forces after the landslide displacement occurs:

$$x'_{B1} = \frac{H_1'}{w_1}\sinh^{-1}\left(\frac{d}{\frac{2H_1'}{w_1}\sinh\left(\frac{w_1(L_1 + \Delta_{LS} - \Delta_{pole})}{2H_1'}\right)}\right) + \frac{(L_1 + \Delta_{LS} - \Delta_{pole})}{2} \quad (25)$$

$$x'_{B2} = \frac{H_2'}{w_2}\sinh^{-1}\left(\frac{d}{\frac{2H_2'}{w_2}\sinh\left(\frac{w_2(L_2 - \Delta_{LS} + \Delta_{pole})}{2H_2'}\right)}\right) + \frac{(L_2 - \Delta_{LS} + \Delta_{pole})}{2} \quad (26)$$

The pole deformation caused by the landslide is equal to the difference in horizontal forces acting on the top of the pole divided by the stiffness of the pole:

$$\Delta_{pole} = \frac{[(H_1' - H_1)n - (H_2' - H_2)n]}{k} \quad (27)$$

where *n* is the number of conductors on either side of the pole. Finally, we solve the five above equations simultaneously to compute the updated horizontal forces in the conductors, H_1' and H_2', and for the pole deformation, Δ_{pole}. In this case, we assume the pole drift threshold requiring the replacement of the pole, PD_R = 0.9 m.

For a given landslide displacement, Δ_{LS}, there is an associated probability that the pole drift will exceed the replacement threshold. This probability is calculated by iterating through the full range of possible pole stiffnesses and determining whether the pole deformation exceeds the replacement threshold, and then weighting those results by the probability of the stiffness. Results are aggregated to determine the total probability that the pole deformation exceeds the replacement threshold for a given landslide displacement, $P(\Delta_{pole} > PD_R | \Delta_{LS})$.

4. LANDSLIDE DISPLACEMENT HAZARD

To determine the frequency with which a given damage state occurs, we must calculate the underlying frequency of the full range of ground deformations that have a finite probability of causing the damage state. We turn to probabilistic landslide hazard analysis which relates ground movement quantities to a frequency of exceedance. Landslide hazard during earthquakes is typically calculated using simplified Newmark sliding block models. The soil block that moves during the landslide is represented by an infinite slope model (Wang 2014), as depicted in Figure 6. The purpose of this model is to calculate the effective ground acceleration, k_y, that will cause the block (or landslide mass) to slide, based on properties of the soil and the slope:

$$k_y = (FS_{static} - 1) g \cdot \sin\alpha \quad (28)$$

where FS_{static} is the factor of safety against sliding in the static case, g is the acceleration due to gravity, and α is the slope angle of the site. FS_{static} is calculated as follows:

$$FS_{static} = \frac{c'}{\gamma \cdot t \cdot \sin\alpha} + \frac{\tan\phi'}{\tan\alpha}\left(1 - m \cdot \frac{\gamma_w}{\gamma}\right) \quad (29)$$

where c' is the effective cohesion of the soil, γ is the unit weight of the soil, *t* is the slope-normal thickness of the block, ϕ' is the effective friction angle of the soil, m is the proportion of the soil block thickness that is saturated, and γ_w is the unit weight of water.

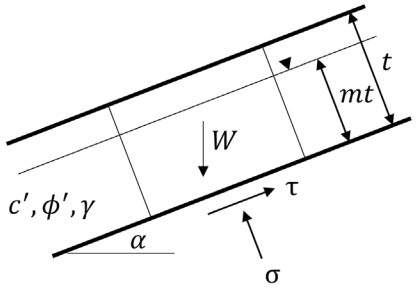

Figure 6. Infinite slope soil model under static conditions.

There are numerous available relationships between earthquake intensity, effective yield acceleration, and landslide displacement that have been developed by performing numerical analysis of slopes with different properties subjected to recorded earthquakes. We have chosen to use the relationship developed by Rathje and Saygili (2009) because it uses peak ground acceleration (PGA) and earthquake moment magnitude (M) to define the intensity of the earthquake, and these parameters and their interrelationship are relatively available across many return intervals in the U.S. using the United States Geological Survey tools. The landslide displacement, Δ_{LS}, is calculated as follows:

$$\ln\Delta_{LS} = 4.89 - 4.85\left(\frac{k_y}{PGA}\right) - 19.64\left(\frac{k_y}{PGA}\right)^2 + 42.49\left(\frac{k_y}{PGA}\right)^3 - 29.06\left(\frac{k_y}{PGA}\right)^4 + 0.72\ln(PGA) + 0.89(M - 6) \quad (30)$$

where the dispersion of the displacement is:

$$\sigma_{\ln \Delta_{LS}} = 0.732 + 0.789\left(\frac{k_y}{PGA}\right) - 0.539\left(\frac{k_y}{PGA}\right)^2 \quad (31)$$

It is important to note that displacement is a function of both PGA and M. The landslide displacement exceedance rate, $\lambda_{\Delta_{LS}}(x)$ for a particular value of displacement, x, is calculated as follows:

$$\lambda_{\Delta_{LS}}(x) = \sum_i \sum_k P[\Delta_{LS} > x | PGA_i, M_k] \cdot P[M_k | PGA_i] \cdot P[PGA_i] \quad (32)$$

where $P[\Delta_{LS} > x | PGA_i, M_k]$ is the probability that the landslide displacement is greater than the value of interest, x, for a value of PGA and M, which is calculated using the $\ln(\Delta_{LS})$ and $\sigma_{\ln \Delta_{LS}}$ calculated for that particular value of PGA and M, and the k_y:

$$P[\Delta_{LS} > x | PGA_i, M_k] = 1 - \Phi\left(\frac{\ln x - \ln \Delta_{LS}}{\sigma_{\ln \Delta_{LS}}}\right) \quad (33)$$

$P[M_k | PGA_i]$ is the probability that an earthquake magnitude M_k occurred given that the PGA = PGA_i. This is calculated from the seismic hazard disaggregation at a particular return period / PGA value. $P[PGA_i]$ is the probability that PGA = PGA_i, which is found using the hazard curve for the site.

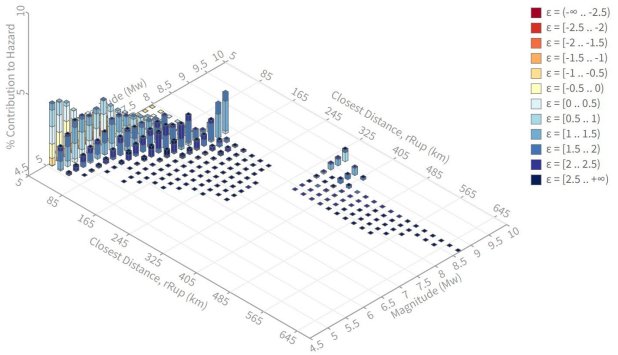

Figure 7. Seismic hazard disaggregation at example location (source: USGS Hazard Tool).

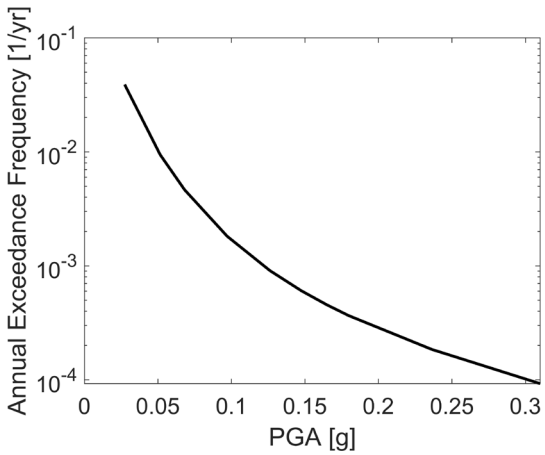

Figure 8. Example hazard curve for PGA.

The rate of exceedance of a particular landslide displacement value is found by conducting numerical integration over the entire range of possible PGA values and M values corresponding to the PGA values. This calculation is repeated for different values of landslide displacement, resulting in a landslide displacement demand curve for a site.

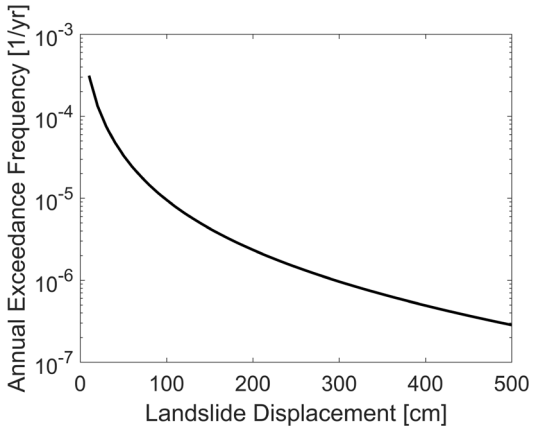

Figure 9. Example landslide displacement demand curve.

5. FAILURE RATES

We calculate the annual rate of pole replacement λ_{PR} by integrating the probability of the pole drift exceeding the threshold for replacement given a landslide displacement (the pole fragility) with the landslide displacement demand curve:

$$\lambda_{PR} = \int_0^\infty P\left(\Delta_{pole} > PD_R | \Delta_{LS}\right) \cdot \left|\frac{\mathrm{d}\lambda_{\Delta_{LS}}}{\mathrm{d}\Delta_{LS}}\right| \mathrm{d}\Delta_{LS} \quad (34)$$

where $P\left(\Delta_{pole} > PD_R | \Delta_{LS}\right)$ is the probability of the pole drift exceeding the threshold for replacement PD_R given landslide displacement Δ_{LS}, and $\lambda_{\Delta_{LS}}$ is the landslide displacement demand curve.

6. EXAMPLE APPLICATION

We demonstrate the utility of the model by calculating the annual failure rate (rate of replacement) of a wood pole in a hypothetical location in California with a relatively steep slope angle = 22 degrees. The slope angle was estimated via linear interpolation of elevation data based on the Digital Elevation Model produced by the U.S. Geological Survey 3D Elevation Program (USGS). We use a California DEM with a 1/3 arc resolution (approximately a 10-meter horizontal resolution).

The effective angle of internal friction of the soil was estimated as 28 degrees based on the soil maps created by the California Soil Resource Lab at the University of California, Davis and the University of California Agriculture and Natural Resources, in collaboration with the US Department of Agriculture (USDA) Natural Resources Conservation Service (Walkinshaw et al. 2022). The maps aggregate USDA soil survey data within 800 m grid cells, and are intended to depict regional trends in soil properties, but may not match the actual data at any given point. A USDA soil texture class is identified at the locations of interest based on the maps, and a corresponding likely soil class was determined according to the Universal Soil Classification System (USCS) and an empirical mapping scheme between USDA texture types and USCS classes developed by the U.S. Army Engineer Research and Development Center (García-Gaines, R. A., & Frankenstein, S. 2015; Carter, M., & Bentley, S. P. 2016).

The USDA soil texture class is based on a thickness-weighted average of the soil either between 0 and 25 cm, or between 25 and 50 cm, whichever yields the most conservative (smallest) angle of internal friction. It is acknowledged that estimates of the soil strength based on the texture of the shallow layers contain significant uncertainties. These estimates may be refined based on detailed geological field studies. The cohesion of the soil is neglected ($c' = 0$). This assumption leads to conservative estimates of the site vulnerability to landslides, but may be refined if more reliable estimates of the soil cohesion are obtained.

In addition to the site properties, disaggregation of the seismic hazard (the probability of each possible earthquake magnitude M given the occurrence of a PGA value of interest) is obtained at the location of interest using the Java-based program nshmp-haz (USGS), which was developed by the National Seismic Hazard Mapping Project within the USGS's Earthquake Hazards Program. The 2018 Conterminous US earthquake source model is employed in the hazard calculations. The earthquake hazard is disaggregated at 10 different PGA levels corresponding to return periods between 25 and 10,000 years. The time-averaged shear-wave velocity in the upper 30 meters (V_{s30}) is 710.1 m/s, which is used in the analysis to obtain site-specific seismic hazard estimates. The Vs30 value was obtained based on the 2018 updated USGS V_{s30} map for California (Thompson, E.M. 2018). An example of the disaggregation of the seismic hazard for a 475-year return period (10% probability of exceedance in 50 years) is shown in Figure 7 and the computed PGA and landslide displacement hazard curves are shown in Figure 8 and Figure 9, respectively.

The hypothetical pole structure is assumed to be 15 m tall with a tapered cross section whose diameter varies between 20 cm at the top and 40 cm at the ground level. The conductor spans on either side of the pole are assumed to be 91 m each, and the number of conductors is assumed to

be three. The conductor weight per unit length is assumed to be 7.3 N/m, and the initial tensile force in the conductor is assumed to be 13.3 kN. Analysis of the pole vulnerability to landslide displacements between 10 and 500 cm leads to an annual failure rate of approximately 0.00001/year. The disaggregation of the failure rate is shown in Figure 10.

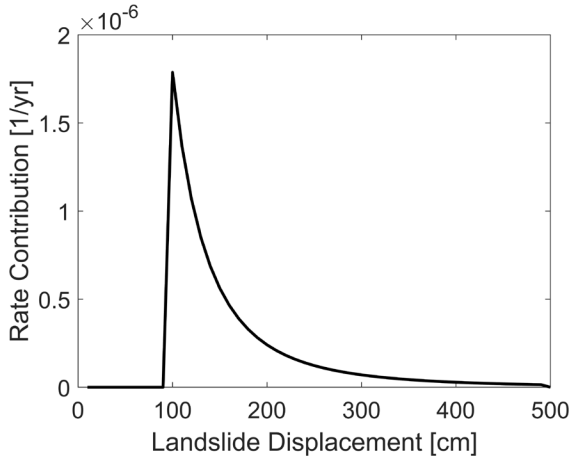

Figure 10: Contribution of different landslide displacements to the failure rate of the example pole.

7. CONCLUSIONS

The proposed model can be used to assess the vulnerability of electric power infrastructure to earthquake-induced landslides. The model relies upon site-specific topographic and seismic hazard information that is available for the continental United States, and can be efficiently estimated across large regional domains. The slope stability analysis underlying the landslide hazard calculations relies on the geotechnical soil properties at the locations of interest, whose estimation is associated with substantial uncertainty and may require site-specific analysis to improve the model predictions. Nonetheless, regional-scale application of the model can capture the infrastructure vulnerability trends based on the region-specific topographic, geotechnical and seismic hazard information. Finally, realistic estimation of the deformations of wood poles and other types of electric infrastructure should account for the impact of aging effects, which may lead to increasing the corresponding probabilities of failure.

8. REFERENCES

Carter, M., & Bentley, S. P. (2016). Soil properties and their correlations. John Wiley & Sons.

García-Gaines, R. A., & Frankenstein, S. (2015). USCS and the USDA soil classification system: Development of a mapping scheme.

Jibson, E. L. & Harp. R. W. (1995). Inventory of landslides triggered by the 1994 Northridge, California earthquake. Inventory of landslides triggered by the 1994 Northridge, California earthquake - ScienceBase-Catalog

Lin, C. W., Shieh, C. L., Yuan, B. D., Shieh, Y. C., Liu, S. H., & Lee, S. Y. (2004). Impact of Chi-Chi earthquake on the occurrence of landslides and debris flows: example from the Chenyulan River watershed, Nantou, Taiwan. *Engineering geology*, *71*(1-2), 49-61.

Rathje, E. M., & Saygili, G. (2009). Probabilistic assessment of earthquake-induced sliding displacements of natural slopes. Bulletin of the New Zealand Society for Earthquake Engineering, 42(1), 18-27.

Thompson, E.M. (2018). An Updated Vs30 Map for California with Geologic and Topographic Constraints (ver. 2.0, July 2022) - ScienceBase-Catalog.

United States Geological Survey (USGS), Datasets (nationalmap.gov)

United States Geological Survey (USGS), https://github.com/usgs/nshmp-haz/wiki

Walkinshaw, M., O'Geen, A.T. & Beaudette, D.E. (2022). "Soil Properties." California Soil Resource Lab: casoilresource.lawr.ucdavis.edu/soil-properties/.

Wang, Y. (2014). Probabilistic assessments of the seismic stability of slopes: Improvements to site-specific and regional analyses. [Doctoral Dissertation, University of Texas at Austin].